Thermoviscoelastic Analysis of the Thermoplastic Composite Tape Placement Process

Fazil O. Sonmez and H. Thomas Hahn

Journal of Thermoplastic Composite Materials 1997; 10; 381
DOI: 10.1177/089270579701000406

Thermoviscoelastic Analysis of the Thermoplastic Composite Tape Placement Process

FAZIL O. SONMEZ* AND H. THOMAS HAHN
Mechanical, Aerospace and Nuclear Engineering Department
University of California, Los Angeles
Los Angeles, CA 90024

ABSTRACT: The thermomechanical behavior of a thermoplastic composite laminate during the tape placement process has been studied. Stresses induced by the compaction roller are predicted using a finite element method. These stresses control the compaction and bonding behavior of the laminate. In the analysis, the tape placement process is considered as a quasi-steady state rolling contact problem. The effect of temperature on creep compliance is included by treating the composite as a thermorheologicaliy simple material. Thermal expansion coefficients are allowed to be temperature dependent. The effect of friction at the contact surface is also taken into account.

The numerical results show how the process parameters (e.g., roller velocity, roller pressure, heat input) are related to temperature and stress distributions within the composite. These relationships can be used to predict the bonding behavior of the laminate.

1. INTRODUCTION

THE INTRODUCTION OF high-performance thermoplastic composites opened the possibility for higher production efficiency, shorter production cycles, and more flexibility in forming techniques. Given these advantages advanced thermoplastic composites also led to new requirements imposed on process conditions. Processing of thermoplastic composites requires much higher temperatures and pressures than thermosets. With shorter process times and higher temperature and stress requirements, determining the correct process parameters and applying them with more precision became more important.

Despite the importance of pressure in achieving consolidation [1], little attention has been paid to the problem of finding the stress distribution within the composite induced by the roller force during the tape placement process. Sarrazin and Springer [2] developed a thermoelastic stress model for tape placement based on FEM. They assumed that the roller is bonded to the laminate along the contact

*Author to whom correspondence should be addressed.

0892-7057/97/04 0381–34 $10.00/0

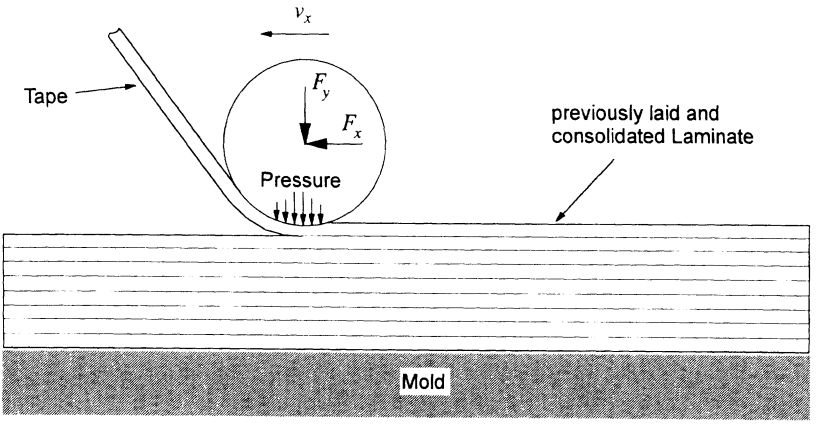

Figure 1. *The tape placement process.*

length and formulated the process as a punch problem rather than a rolling contact problem. They also did not consider the boundary between the tape and the substrate. They assumed that the incoming tape is bonded to the substrate.

Polymer composites display viscoelastic behavior at medium to high temperatures. In this study, therefore, the process is considered as a viscoelastic rolling contact problem. Formulation of the problem is based on work by Lynch [3] and Batra et al. [4]. A schematic description of the system to be analyzed is shown in Figure 1. Stresses and strains are induced by roller indentation and thermal expansion. During the process, the material experiences a large temperature change. On that account, the effect of temperature on creep compliance and thermal expansion coefficients is included. Coulomb's dry friction law is used to describe the phenomenon of friction between the roller and the laminate.

The literature includes numerous analytical studies of viscoelastic rolling contact problems. Hunter [5] and Morland [6] solved the rolling contact problem involving a rigid cylinder, rolling over a viscoelastic half-space. Margetson studied indentation of a viscoelastic strip between rotating rigid cylinders [7] and rolling over a viscoelastic layer [8]. Morland [9], Kalker [10], Wang [11], and Wang and Knothe [12] considered the rolling contact between two viscoelastic cylinders.

The inherent complexity of the problem forces the use of numerical methods. Lynch [3] solved the viscoelastic rolling contact problem by FEM without including thermal effects. Numerical results agreed well with the experimental data obtained by photoviscoelastic measurements. Batra and his coworkers used a similar approach to study the problems of the indentation of a rubber-covered roll [4] and a viscoelastic sheet [13] by a rigid cylinder. They also included thermal effects. However, they allowed the temperature change only through the thickness of the sheet so that no heat transport was allowed in and out of the control volume. Besides, they neglected the effect of temperature on thermal expansion coefficients. They also assumed frictionless contact. Later, Bapat and Batra [14] solved the

rubber-covered roll problem by a nonlinear finite element method. Oden and Lin [15] used FEM to study the general geometrically nonlinear rolling contact of viscoelastic cylinders. In all of these studies, the material was assumed to be isotropic.

2. FORMULATION OF THE PROBLEM

2.1 Equilibrium Equations

Normally, tape placement is a 3D process. However, in order to simplify the analysis, the most basic lay-up geometry is chosen. The plate is assumed to be a flat unidirectional laminate made of the same composite. The width of the laminate is small and the same as that of the roller, so that a plane stress state is assumed (Figure 2). Depending on the thickness of the laminate, plane strain may also be assumed.

The roller moves with a constant velocity v_x, which is presumed to be sufficiently small so that all inertial effects are negligible. A steady state is assumed to apply within the Eulerian control volume moving with the roller away from the edges. Previous studies showed [3,13] that the stress field was quite concentrated under the roller and quickly decayed to zero as the distance from the roller increased. Experimental studies of tape placement also do not show any quality difference along the length of the laminate. It can then be concluded that process conditions along the path of the roller do not vary, and the steady state assumption holds except at locations very near the edges.

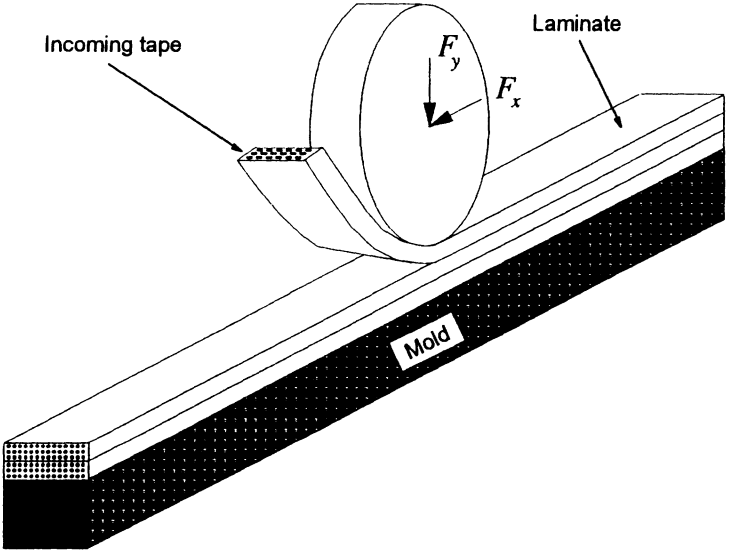

Figure 2. *Analyzed configuration of the process.*

Neglecting the inertial forces, the equilibrium equations for two-dimensional analysis become

$$\frac{\partial \sigma_1}{\partial x}+\frac{\partial \sigma_6}{\partial y}=0$$
$$\frac{\partial \sigma_6}{\partial x}+\frac{\partial \sigma_2}{\partial y}=0 \tag{1}$$

2.2 Constitutive Relations

In the analysis, linear constitutive relations are used. Displacement gradients $u_{i,j}$ are in absolute value much smaller than unity. Namely, the displacement changes slowly within the control volume. Displacement components u_i are also small with respect to the roller diameter when the coordinate axes are fixed to the roller. Material nonlinearity is also assumed to be negligible. In press molding, the recommended stress level for consolidation is between 1 and 2 MPa [16]. For APC-2, the transverse stress-strain curve is linear up to 25 MPa at 150°C [17]. Although in the tape placement process, higher consolidation stresses are required due to shorter bonding times, linear constitutive relations can be used without any significant loss in accuracy.

In comparison to the amount of heat supplied to melt the material, mechanical heating through deformation is negligible. Thus, thermal and mechanical analyses are carried out separately.

For a continuous unidirectional fiber-reinforced composite having a viscoelastic matrix, the creep compliances S_{11} and S_{12} can be taken to be independent of time and temperature [18,19], where the fibers are in the "1" direction. Bearing in mind that the plane of the transverse isotropy is a "2-3" plane, constitutive relations for a transversely isotropic viscoelastic laminate in plane stress are expressed as [20–22]

$$\varepsilon_1(t)-\varepsilon_1^*(t)=S_{11}\sigma_1(t)+S_{12}\sigma_2(t)$$
$$\varepsilon_2(t)-\varepsilon_2^*(t)=S_{12}\sigma_1(t)+\int_0^t S_{22}(\xi-\xi')\frac{\partial \sigma_2(\tau)}{\partial \tau}d\tau \tag{2}$$
$$\varepsilon_6(t)=\int_0^t S_{66}(\xi-\xi')\frac{\partial \sigma_6(\tau)}{\partial \tau}d\tau$$

where $\varepsilon_i^*(t)$ is the thermal strain. Since the thermal expansion coefficients are temperature dependent, they are given by

$$\varepsilon_i^*(t) = \int_{T_o}^{T_f} \alpha_i(T)\,dT \tag{3}$$

ξ is the pseudo time, which explains the temperature dependence of the creep compliance. It is given by

$$\varepsilon = \int_0^t a[T(\eta)]\,d\eta \tag{4}$$

$a(T)$ is the shift factor, which is related to the amount of horizontal shift required to make the modulus-time curve for the temperature T coincide with the one corresponding to the base temperature T_{base}.

2.3 Boundary Conditions

The roller and the mold are assumed to be made of considerably harder material than the composite undergoing processing. Therefore, they are considered to be rigid.

The friction coefficient at the contact surface is about 0.24 [23]. Hahn and Levinson [24] showed that the effect of the frictional force at the contact surface could be significant for this level of friction coefficient. Therefore, the effect of friction is included in the stress analysis. Coulomb's friction law with a constant coefficient of friction is used. No differentiation is made between the adhesion, slip or partial slip phenomenon.

Normally a force is applied to the tape in order to open the interface. However, this force should be small. Excessive forces on the tape induce high shear stresses at the tape-substrate interface and thus cause delamination. Therefore, the force applied to the tape is neglected.

On the top surface, we have the following boundary conditions:

$$u_y(x,0) = d + \sqrt{R^2 - [x + u_x(x,0)]^2} - R \rightarrow \text{in contact with the roller}$$

$$F_s = F_r \mu \tag{5}$$

$$\sigma_{ji} n_j = 0 \qquad \rightarrow \text{not in contact with the roller}$$

where d is the depth of indentation (Figure 3), R is the radius of the roller, u_x and u_y are the x and y components of the displacement, respectively, n_j is the outward directed unit normal to the surface, F_r and F_s are the normal and frictional forces, respectively, and μ is the coefficient of friction at the contact surface. The first condition states that the deformed shape of the contact surface conforms to the circular shape of the rigid indentor, while the second condition comes from the Coulomb's

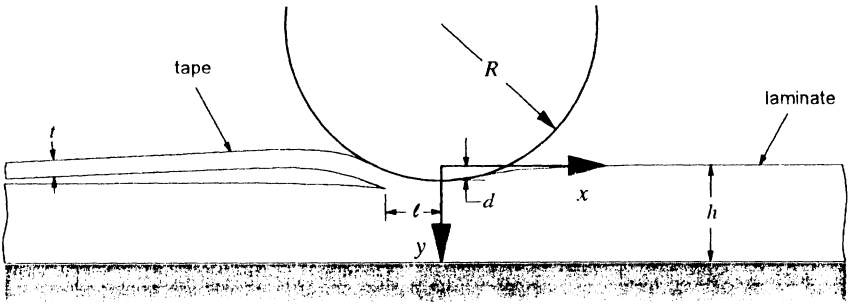

Figure 3. *Configuration of the contact surface.*

friction law. The third condition indicates that when the top surface is not in contact with the roller, it is traction free.

The bottom of the tape and the top of the laminate up to the nip point are traction free.

$$\sigma_{ji} n_j = 0 \qquad y = t, \quad x < -l \tag{6}$$

The laminate is assumed to be perfectly bonded to the rigid mold. Therefore, at the bottom surface, the following boundary conditions are met:

$$\left.\begin{aligned} u_y &= 0 \\ u_x &= 0 \end{aligned}\right\} \quad y = h \tag{7}$$

where h is the thickness of the laminate.

The control volume is sufficiently large so that the material entering or exiting from the control volume is stress free.

Normal stress on the contact surface is continuous, and hence it vanishes at the ends of the contact area.

3. FINITE ELEMENT SOLUTION OF THE PROBLEM

3.1 Formulation

The portion of the laminate to be analyzed is divided into eight-degrees-of-freedom rectangular elements concentrated under the roller as shown in Figure 4. The position of the tape is horizontal in the undeformed shape.

The strain in a finite element is a linear function of the eight nodal displacements [25] as in the elastic analysis:

$$\{\varepsilon\}_r = [A]_r \{\delta\}_r \tag{8}$$

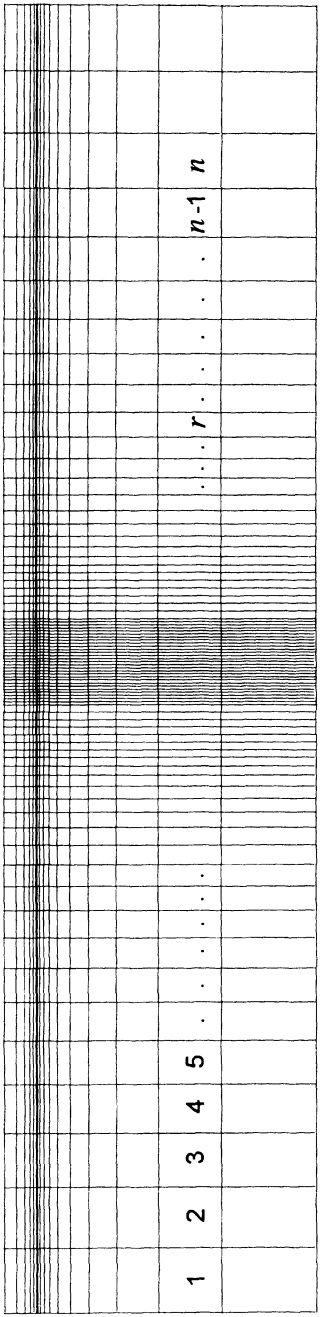

Figure 4. *Mesh structure used in the stress analysis. Horizontal and vertical dimensions are not on scale.*

where $[A]_r$ is a 3 × 8 matrix whose elements depend only on the nodal displacements of the element r, $\{\delta\}_r$.

The viscoelastic memory of the material is reflected by the stress state in a given element being influenced by the strains in all the elements through which the material passed previously. Considering the quasi-steady state assumption, in which the stress and strain state in the control volume does not change with time, the strain history of a material occupying a particular element can be estimated from the current configuration. For example, the material occupying the element n (Figure 4) was in the elements 1,2,3, . . .,$n-1$ at times, $t_1,t_2,t_3, \ldots,t_{n-1}$ and had the same stress and strain state as the materials occupying these elements at the present time. It should also be noted that moving of the tape up or pushing of the roller into the laminate do not constitute part of the viscoelastic history the material experiences. As shown in Figure 5, a material point follows the path that corresponds to the deformed shape of the horizontal strip containing that material point. Thus, the stress components in the finite element n (Figure 4) are found by adding the contributions by all the elements through which the material has previously passed. This can be done by converting the convolution integrals in Equation (2) into a summation of series and reducing the relation to the following form (Appendix A):

$$\begin{Bmatrix} \sigma_1^n \\ \sigma_2^n \\ \sigma_6^n \end{Bmatrix} = \sum_{r=1}^{n} \begin{bmatrix} c_{11}^{nr} & c_{12}^{nr} & 0 \\ c_{12}^{nr} & c_{22}^{nr} & 0 \\ 0 & 0 & c_{66}^{nr} \end{bmatrix} \begin{Bmatrix} \varepsilon_1^r - \varepsilon^{*r}_1 \\ \varepsilon_2^r - \varepsilon^{*r}_2 \\ \varepsilon_6^r \end{Bmatrix} \tag{9}$$

or more concisely

$$\{\sigma\}_n = \sum_{r=1}^{n} [C]_{nr} \{\varepsilon\}_r - \sum_{r=1}^{n} [C]_{nr} \{\varepsilon^*\}_r \tag{10}$$

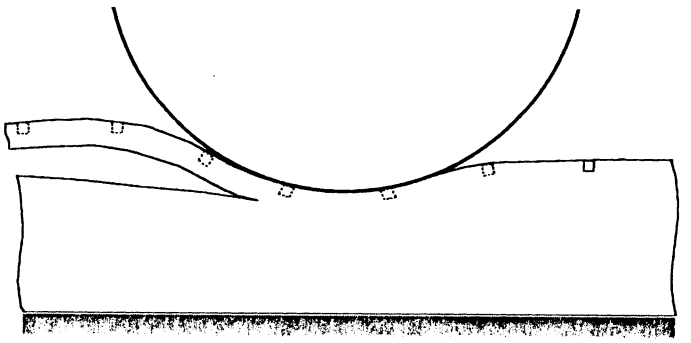

Figure 5. *Path of a material point following the deformed shape of the horizontal strip.*

where $\{\varepsilon^*\}_r$ is the thermal strain vector (Appendix B) whose elements depend only on the nodal temperatures of the element r. Combining Equations (8) and (10), we get

$$\{\sigma\}_n = \sum_{r=1}^{n} [C]_{nr} [A]_r \{\delta\}_r - \sum_{r=1}^{n} [C]_{nr} \{\varepsilon^*\}_r \tag{11}$$

Unlike the elastic case in which the element stresses depend only on the nodal displacements of that particular element, in the present viscoelastic analysis they are functions of the nodal displacements of all the preceding elements in the same horizontal strip. Consequently, the band width of the resulting global stiffness matrix is much larger, and the computational time is much longer than the elastic case.

The virtual work principle is written as

$$\{\delta\}_n^T \{F\}_n = \int_{V_n} \{\varepsilon\}_n^T \{\sigma\}_n \, dV_n \tag{12}$$

where $\{F\}_n$ is the vector of forces acting at the nodal points of the element n, and V_n is its volume. Substituting Equation (8) and Equation (11) into Equation (12), we have

$$\{\delta\}_n^T \{F\}_n = \int_{V_n} \{\delta\}_n^T [A]_n^T \left[\sum_{r=1}^{n} [C]_{nr} [A]_r \{\delta\}_r - \sum_{r=1}^{n} [C]_{nr} \{\varepsilon^*\}_r \right] dV_n \tag{13}$$

By equating the terms in front of the nodal displacement vector $\{\delta\}$, we obtain

$$\{F\}_n = \int_{V_n} \sum_{r=1}^{n} [A]_n^T [C]_{nr} [A]_r \{\delta\}_r \, dV_n - \int_{V_n} \sum_{r=1}^{n} [A]_n^T [C]_{nr} \{\varepsilon^*\}_r \, dV_n \tag{14}$$

or,

$$\{F\}_n = \sum_{r=1}^{n} [K]_{nr} \{\delta\}_r + \sum_{r=1}^{n} \{H\}_{nr} \tag{15}$$

Here $[K]_{nr}$ is the effective element stiffness matrix given by

$$[K]_{nr} = \int_{V_n} [A]_n^T [C]_{nr} [A]_r \, dV_n \tag{16}$$

and, $[H]_{nr}$ is the effective thermal force vector.

$$\{H\}_{nr} = -\int_{V_n} [A]_n^T [C]_{nr} \{\varepsilon^*\}_r \, dV_n \tag{17}$$

Components of the element stiffness matrix and the thermal force vector are given in Reference [26]. Assembling all the element stiffness matrices and the thermal force vectors for the entire control volume, we obtain

$$\{F\} = [K]\{\delta\} + \{H\} \tag{18}$$

where $[K]$ is the $(2\,m \times 2\,m)$ global stiffness matrix, m being the number of nodes, $\{F\}$ is the force vector, $\{\delta\}$ is the displacement vector, and $\{H\}$ is the thermal force vector. The factor 2 indicates the two degrees of freedom at each node. The global stiffness matrix $[K]$ is unsymmetric and banded.

Equation (18) is the equilibrium equation to be solved together with the boundary conditions. First Equation (18) is rearranged as

$$\begin{Bmatrix} F_f \\ F_r \end{Bmatrix} = \begin{bmatrix} K_{ff} & K_{fr} \\ K_{rf} & K_{rr} \end{bmatrix} \begin{Bmatrix} \delta_f \\ \delta_r \end{Bmatrix} + \begin{Bmatrix} H_f \\ H_r \end{Bmatrix} \tag{19}$$

where the subscript r represents the restrained degrees of freedom, while f denotes the free ones. Since

$$\{\delta_r\} = \{0\} \tag{20}$$

the final system of equations to be solved becomes

$$\{F_f\} = [K_{ff}]\{\delta_f\} + \{H_f\} \tag{21}$$

3.2 Solution

3.2.1 DETERMINING THE DEFORMED SHAPE OF THE CONTACT SURFACE

In order to solve Equation (21), in which neither the force nor the displacement vector is known, the iterative procedure reported by Batra et al. [4] is modified to determine the contact forces.

The procedure is summarized in Figure 6. First, we assume an arc of contact, along which distributed loads are expressed in terms of concentrated loads at the nodal points. Frictional forces are then calculated using Coulomb's friction law.

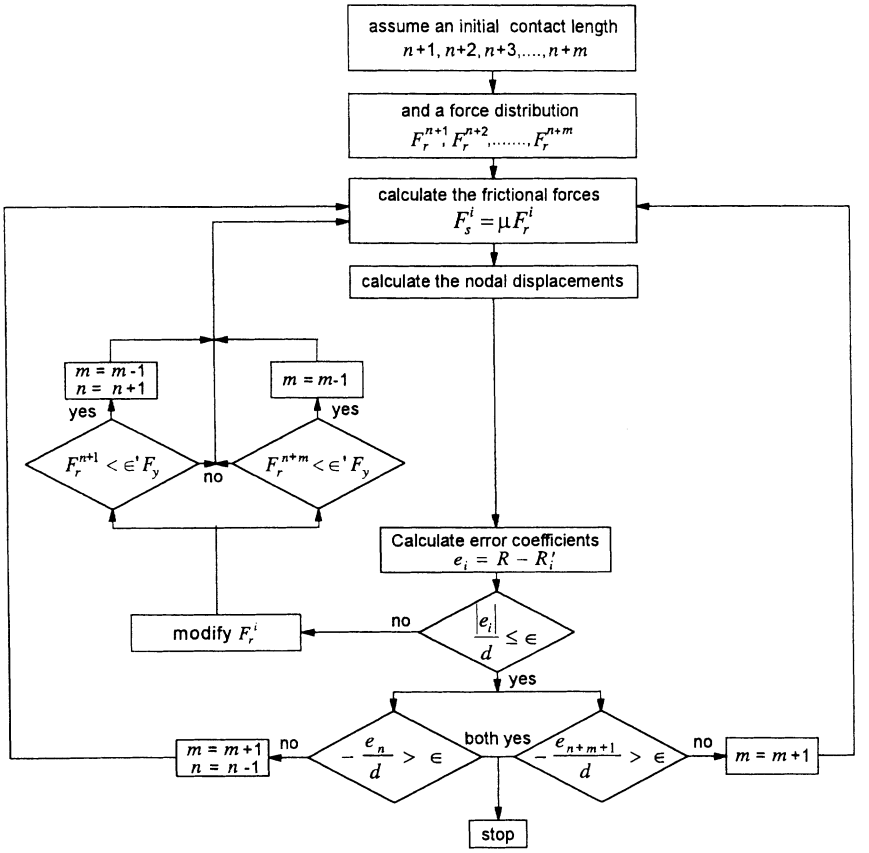

Figure 6. *The procedure used in estimating the contact length and the contact force distribution.*

Given the nodal forces, nodal displacements are calculated from Equation (21) using the triangulation method [27]. Having solved for the displacements corresponding to the assumed force distribution, a check is made, first to the deformed surface whether it conforms to the circular profile of the roller, second to the length of the assumed arc of contact. Should the deformed contact surface not match the shape of the roller, the loads on the contact surface are adjusted in the manner detailed below, and Equation (21) is solved again.

To perform the above-mentioned check and adjust procedure, we proceed as follows: The nodes in contact with the roller are numbered as $n+1, n+2, n+3, \ldots n+m-1, n+m$, where m is the number of nodes in contact starting with the node number $n+1$. The node through which the y axis passes is chosen to be the center point and called c. The R_i' is defined as the distance between the center of the roller and the node i on the contact surface as shown in Figure 7.

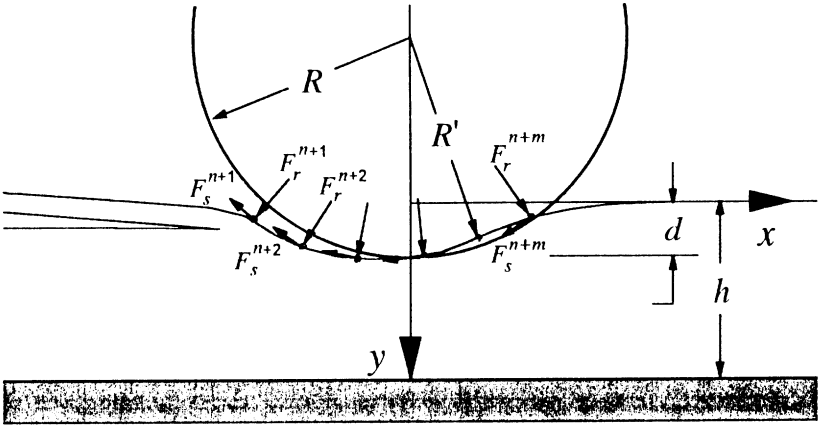

Figure 7. *Configuration of the contact area.*

$$R_i' = \sqrt{(R - d + u_y^i)^2 + (x_i + u_x^i)^2} \tag{22}$$

where u_y^i is the y component of the nodal displacement i, u_x^i is the x component, and the identation d is equal to u_y^c (vertical displacement of the center node). If perfect match occurs, R_i' becomes equal to R at every node on the contact surface. The discrepancy is represented by error coefficients e_i, defined as

$$e_i = R - R_i' \tag{23}$$

We consider that the nodes $n+1, n+2, \ldots, n+m$ lie on the roller surface within an acceptable tolerance, if the following condition is satisfied:

$$\frac{|e_i|}{d} \leq \in \quad i = n+1, n+2, \ldots, n+m \tag{24}$$

where $\in$ is an appropriately chosen small positive number. If the above condition is not satisfied by any one of the nodes, normal forces for the next iteration are calculated by the following equation:

$${}^{q+1}F_r^i = {}^qF_r^i \left(1 + g\frac{e_i}{d}\right) \tag{25}$$

where q is the iteration number and g is a convergence factor. If g is too small, convergence will be very slow. On the other hand, if it is too large, convergence

may not be achieved. For this reason, g is dynamically varied during the iterative process depending on the ratio of e_i/d.

If the forces at the end nodes of the contact area become smaller than a specified value, these nodes are considered not to be in contact with the roller:

$$F_r^i < \in' F_y \quad \text{for} \begin{cases} i = n+1 \\ i = n+m \end{cases} \tag{26}$$

where F_y is the total contact force in the y-direction. If the above condition holds, the corresponding node is removed from the contact surface.

Friction forces at the contact surface are calculated from Coulomb's friction law:

$$^{q+1}F_s^i = {}^{q+1}F_r^i \mu \tag{27}$$

Nodal forces are then calculated from geometry:

$$F_y^i = \frac{R - d + u_y^i}{R_i'} F_r^i + \frac{x_i + u_x^i}{R_i'} F_s^i \tag{28}$$

$$F_x^i = \frac{x_i + u_x^i}{R_i'} F_r^i - \frac{R - d + u_y^i}{R_i'} F_s^i \tag{29}$$

The above procedure is repeated until the condition in Equation (24) is satisfied for every node in contact.

Then, the assumed contact length is checked for smallness. If the nodes adjacent to the contact boundary are far enough from the roller, the arc of contact is considered to be correct.

$$-\frac{e_i}{d} > \in \quad \text{for} \begin{cases} i = n \\ i = n+m+1 \end{cases} \tag{30}$$

If the above condition is not satisfied for any one of these nodes, the contact area is extended to include the corresponding node(s), and the whole procedure is repeated.

After the contact forces and the displacements $\{\delta_f\}$ are determined, the restraint forces corresponding to the constrained degrees of freedom can be calculated from Equation (19):

$$\{F_r\} = [K_{rf}]\{\delta_f\} + \{H_r\} \tag{31}$$

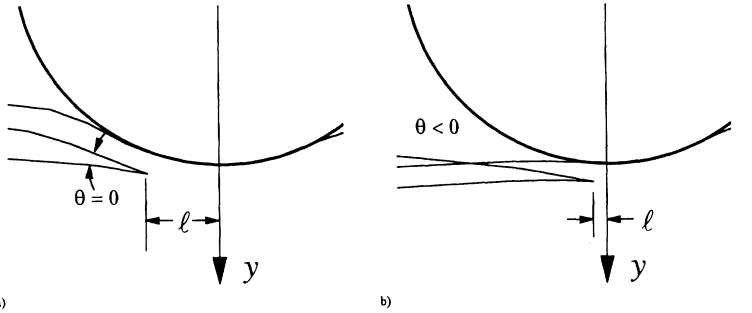

Figure 8. *Determining the location of the nip point; (a) l corresponds to the exact location of the nip point; (b) l is too small.*

3.2.2 DETERMINING THE LOCATION OF THE NIP POINT

Finally, the location of the nip point where the tape and the substrate merge is checked. The exact location depends on the deformed shape of the composite, which is not known at the beginning. Initially a suitable distance, l, between the y-axis and the nip point is assumed, and the deformed shape is determined by following the aforementioned procedures. If the resulting angle between the tape and the laminate, θ, is equal to zero, the distance is considered to be correct [Figure 8(a)]. In this case, normal stress at the nip point also becomes zero. If the angle is less than zero, which is physically not possible, the distance l is smaller than the correct one [Figure 8(b)]. The angle θ also cannot be more than zero. Full bond strength at the tape-laminate interface is not achieved instantaneously. Therefore, the interface cannot sustain tensile forces at the nip point. In the case of non-zero θ, the location of the nip point is modified and the above calculations are repeated. The iterations are continued until the angle θ becomes zero within an acceptable tolerance. If the angle θ is between 0.0 and 3.0 E-3, this requirement is assumed to be met. However, the solution may not be unique due to large thermal stresses. In this case, the correct location of the nip corresponds to the smallest l that satisfies the zero-angle requirement.

3.2.3 SOLUTION PROCEDURE

Figure 9 shows the solution procedure used in the analysis. The thermal and stress analyses are fully coupled. The temperature field generated by the thermal analysis is used in the stress analysis to calculate thermal strains and shift factors. The contact length under the roller determined by the stress analysis is used as a boundary condition in the thermal analysis. Since a different kind of mesh structure is utilized in the stress analysis, the temperature field determined by the thermal analysis is mapped to the grid used in the stress analysis by linear interpolation. Besides, the y axis in the stress analysis passes through the center of the roller, whereas in the thermal analysis, it passes through the nip point. The distance between them is l as shown in Figure 8. Every time l changes during the iterations, the thermal analysis is repeated due to the changed boundary condition to calculate the new temperature distribution, which is then remapped. The stress analysis prob-

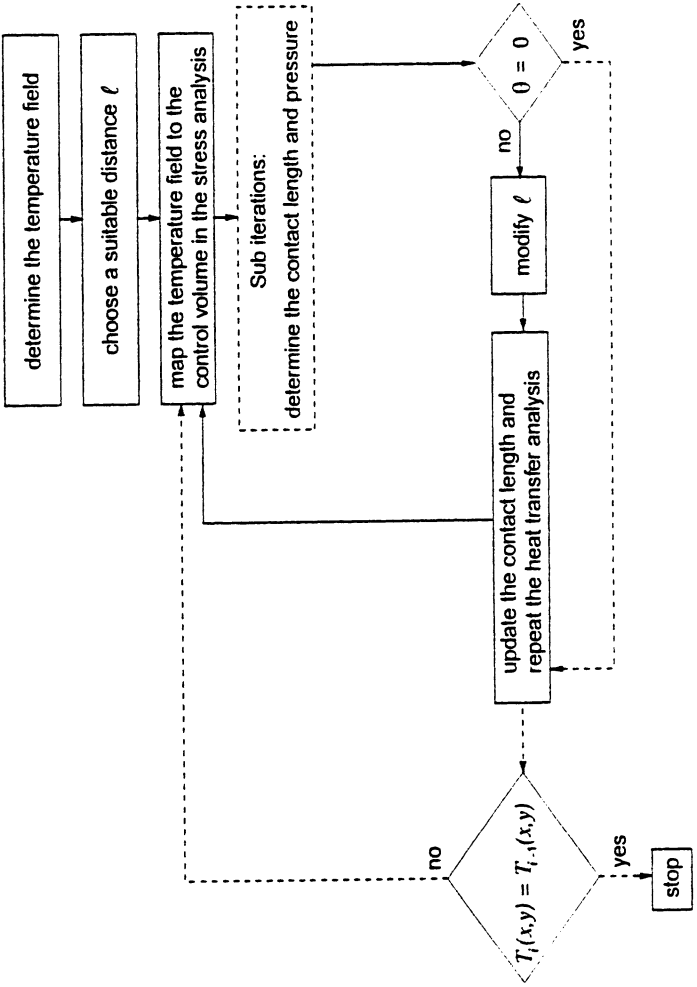

Figure 9. *The solution procedure.*

lem is solved again using the new temperature field. This iterative process is continued until θ becomes zero, and the difference in temperature field obtained in two consecutive iterations becomes negligibly small.

4. RESULTS AND DISCUSSIONS

A computer code was developed following the aforementioned solution procedure, and the effects of the processing parameters on the stress field within the laminate were investigated. The processed material was chosen to be APC-2.

4.1 Verification

The model is verified first by comparing the results with an analytical solution for a simpler problem. Margetson [7] solved the problem of the indentation of a viscoelastic strip between two rotating rigid cylinders. This is mathematically the same as the rolling of a rigid cylinder over a viscoelastic strip with half thickness resting on a frictionless base. The material was isotropic in plane strain. The strip is under homogeneous temperature field. Input parameters are given in Table 1. Figure 10 shows the non-dimensional contact pressure $P(X)$ distribution for two different sheet thicknesses. Analytical and numerical results agree well. The pressure distribution at the contact surface is not symmetric about the center line of the roller, which is characteristic of viscoelastic contact problems. As expected, the contact pressure goes to zero at the ends of the contact area as the traction-free zone is approached.

Second, verification of the code is done by examining the convergence of the results. Convergence of the normal stress at the interface with zero abscissa ($x = 0, y = t$) is shown in Figure 11. Due to very high temperature gradients at the interface, convergence is achieved at large node numbers. However, about 1000 nodes yield acceptable accuracy.

When the initial and infinite values of the creep compliance are the same ($S_0 =$

Table 1. Input parameters for the viscoelastic sheet rolling problem.

Shear modulus (2G)	$G_1 = G_0(1+e^{-t/\tau})$	
Radius of the roller	$R = 1000a$	
Non-dimensional position	$X = x/a$	
Non-dimensional pressure	$P(X) = R(1-\nu)p(X)/aG_0$	
Roller velocity	$v = a/2\tau$	
	$a = b$	**$a = 2.5b$**
a, Half contact length	0.01055	0.013125
b, Sheet thickness	0.01055	0.033
ν, Poisson's ratio	0.25	0.25
Relaxation time	0.5	0.5
G_0	1.0 E6	1.0 E6

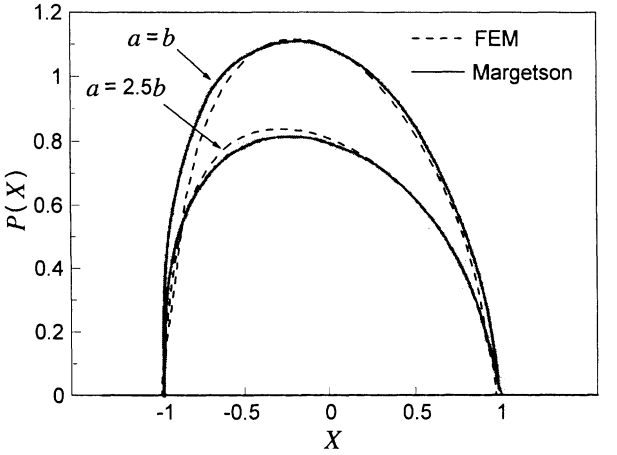

Figure 10. *Comparison between the numerical and the analytical results. P(X) is the non-dimensional contact pressure distribution at the contact surface.*

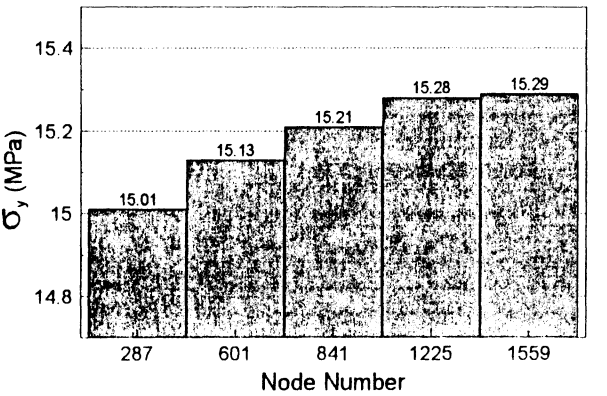

Figure 11. *Convergence of the normal stress at the interface (x = 0, y = t).*

S_∞), identical results are obtained for elastic and viscoelastic analyses. Elastic analysis was verified by comparing the results to the ones generated by an available commercial FEM software (SAP90). The displacement and stress fields generated by both computer codes were the same.

Assuming that the material is thermorheologically simple and temperature field is homogeneous, the pseudo time ξ can be related to the real time by $\xi = ta(T)$ so that relaxation modulus is given by $C(T,t) = C(T_{base}, \xi)$. This means that the effect of temperature on relaxation processes is expressed in terms of the base temperature and a new time scale which itself depends on that temperature. For example, the stress and deformation fields for temperature field $T(x,y) = T_1$ and roller velocity $v_x = v_1$ should be identical to the ones for $T(x,y) = T_{base}$ and $v_x = v_1/a(T_1)$. The computer code also yields the same result for both cases as predicted.

In conclusion, evaluation of the developed computer code by various verification methods indicates the accuracy of the results.

4.2 Inputs for the FEM Code

The viscoelastic behavior of APC-2 has been extensively studied by a number of researchers [17–19, 28–37]. Xiao [18] provided the data regarding the creep compliances and the shift factors. Barnes [38,39] characterized the anisotropic thermal expansion behavior of APC-2. These data together with other program inputs are given in Table 2. Briscoe [23] reported the friction coefficient of a contact formed by a steel ball moving with a sliding velocity 0.45×10^{-3} m/s over a flat specimen of polyetheretherketone as a function of temperature. The value of the coefficient of friction is then chosen based on the temperature at the contact surface. The base temperature, T_{base}, which is used for calculating thermal strains, is taken to be the same as the preheat temperature of the laminate.

Input parameters for the thermal analysis are given in Reference [41]. Also 0.01% degradation criteria is used, and heat input is accordingly selected.

Figure 12 shows the normal stress distribution at the tape-substrate interface as estimated by the elastic and viscoelastic analyses. It also depicts the temperature profile at the interface. The elastic analysis predicts higher and more concentrated normal stresses. Also, the nip point as predicted by the elastic analysis is closer to the y axis.

The stress profile under the roller is very concentrated. After the roller passes, compressive stresses return immediately to zero values or even turn into tension, while the temperature of the material is still above the melting point. In this case, voids will form in the composite due to condensation of air predissolved in the polymer matrix [42]. However, pressure should be maintained until the material cools down to the glass transition temperature [43,44]. This could be achieved by installing a secondary roller or a compaction shoe to the tape placement head. The exact location of the secondary roller can be determined from the model.

4.3 The Effect of Roller Radius

Figure 13 shows the stress distribution at the interface for various roller radii. As

Table 2. Inputs for the computer code.

Material Properties		
Creep Compliance		
S_{11} [40]	7.39×10^{-12} Pa^{-1}	
S_{12} [40]	-2.51×10^{-12} Pa^{-1}	
	$S(t) = S_0 + \dfrac{S_\infty - S_0}{(1+\tau_0/t)^n}$	
S_{22} [18]	S_0	0.103×10^{-9} Pa^{-1}
	S_∞	0.141×10^{-9} Pa^{-1}
	τ_0	1.236×10^{5} sec
	n	0.215
S_{66} [18]	S_0	0.189×10^{-9} Pa^{-1}
	S_∞	0.335×10^{-9} Pa^{-1}
	τ_0	1.8066×10^{5} sec
	n	0.230
Shift Factor		
	$\ln a_T = -\dfrac{\Delta H}{R}\left(\dfrac{1}{T} - \dfrac{1}{T_{base}}\right)$	
$a_T(S_{22})$ [18]	T_{base}	370°K
	ΔH	28.4×10^{3} cal mol^{-1} ($T < T_{base}$)
		86.8×10^{3} cal mol^{-1} ($T < T_{base}$)
	T_{base}	370°K
	ΔH	9.9×10^{3} cal mol^{-1} ($T < T_{base}$)
		57.0×10^{3} cal mol^{-1} ($T > T_{base}$)
R, universal gas constant		1.98 cal K^{-1} mol^{-1}
Thermal expansion coefficients [38,39]		
α_{11} Temperature dependent values		References [38,39]
Average value		0.2×10^{-6}/°C
α_{22} Temperature dependent values		References [38,39]
Average value		58×10^{-6}/°C
Friction coefficient, μ [23] (Temperature dependent)		
Room temperature value		0.24

Table 2. (continued).

Geometry of the Specimen	
Thickness of the tape, t	0.125 mm
Thickness of the laminate, h	2.625 mm
Width of the tape, w	6 mm
Radius of the roller, R	40 mm
Experiment Variables	
Total vertical force applied on the roller, F_y	40 N
Velocity of the roller, v_x	0.01 m/sec
Program Variables	
Length of the strip to be analyzed	0.02 m
Total number of nodes used	1758
Number of divisions through the length of the strip	86
Number of divisions through the thickness of the strip	19
Maximum aspect ratio	10
Base temperature T_0 for thermal expansion	423°K
$\in$ error coefficient	1.0 E-4
$\in'$ error coefficient	5.0 E-6

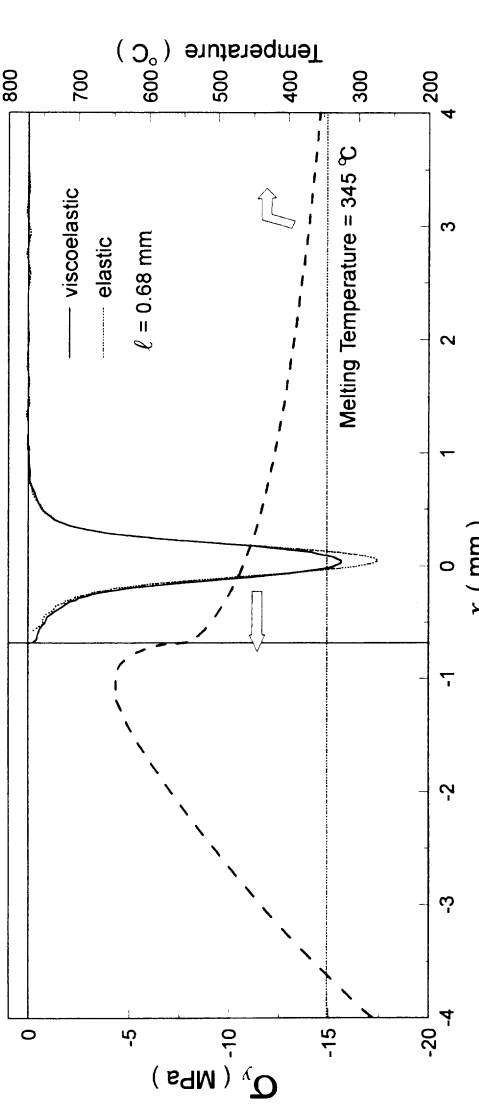

Figure 12. *Normal stress distribution at the tape-laminate interface. Comparison of the elastic and viscoelastic results.*

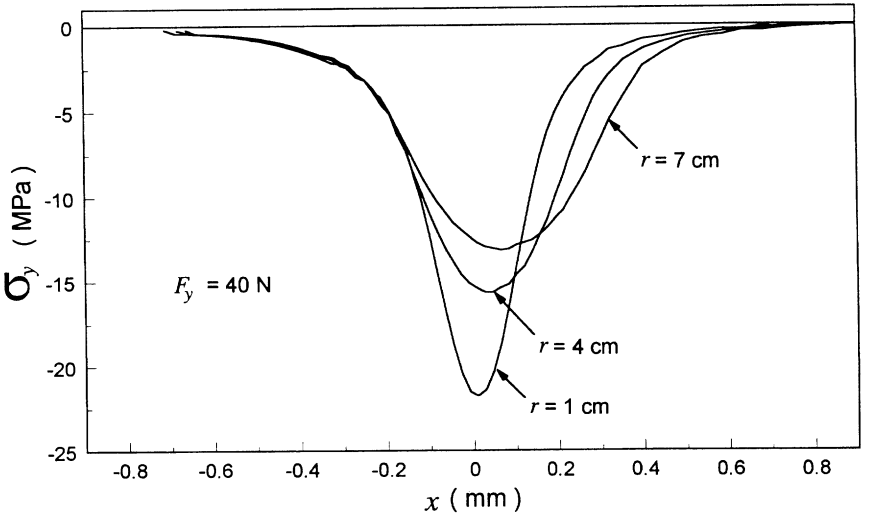

Figure 13. *The effect of roller radius on the stress distribution at the interface.*

the roller diameter gets smaller, stresses become higher and more concentrated. High stresses could cause the fibers to wrinkle and spread [45]. If the stress profile under the roller is very concentrated, the time spent under high stresses will be shorter. Bonding could then be incomplete. Therefore, larger roller diameters are better for consolidation.

4.4 The Effect of Roller Velocity

Figure 14 shows the normal stress distribution at the tape-substrate interface for various roller speeds. The differences in the stress fields are small for the given material properties and process parameters. This means that when the velocity is lower, the interface will experience high stresses for longer times. Then, consolidation is expected to be more complete at low speeds.

When the corresponding temperature profiles are also considered, a different picture arises. As seen in Figures 12, 15 and 16, at high speeds there is more room to increase temperature. Low speeds are more likely to result in thermal degradation due to longer times spent at high temperatures. The resulting interface temperature is thus lower under the 0.01% weight loss criterion. For the roller speed 0.002 m/s, the average temperature experienced by the interface under the roller-induced high stresses is almost below the processing temperature of the polymer. Since, at low temperatures, viscosity of the polymer is lower and diffusion of molecular chains slow, consolidation is achieved at longer times. Low speeds may then lead to incomplete consolidation and high void content.

4.5 The Effect of Laminate Thickness

It should be noted that nowhere in the analysis, has any assumption on the

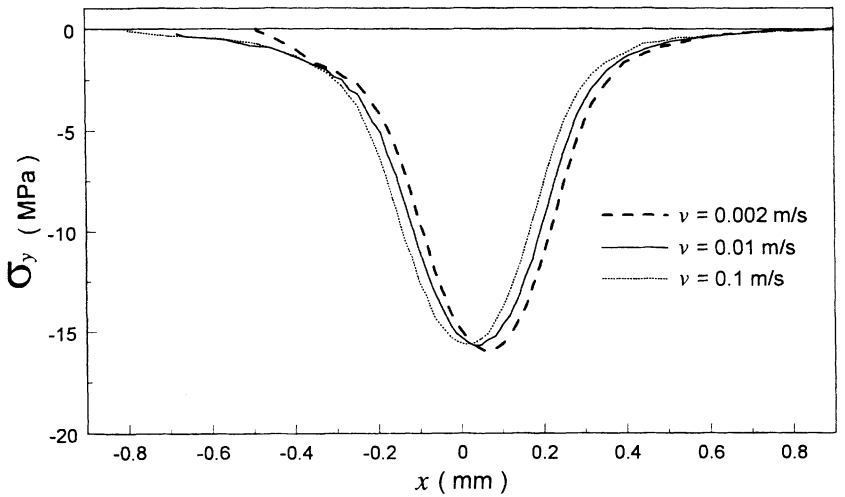

Figure 14. *Stress distributions at the tape-laminate interface for various roller speeds.*

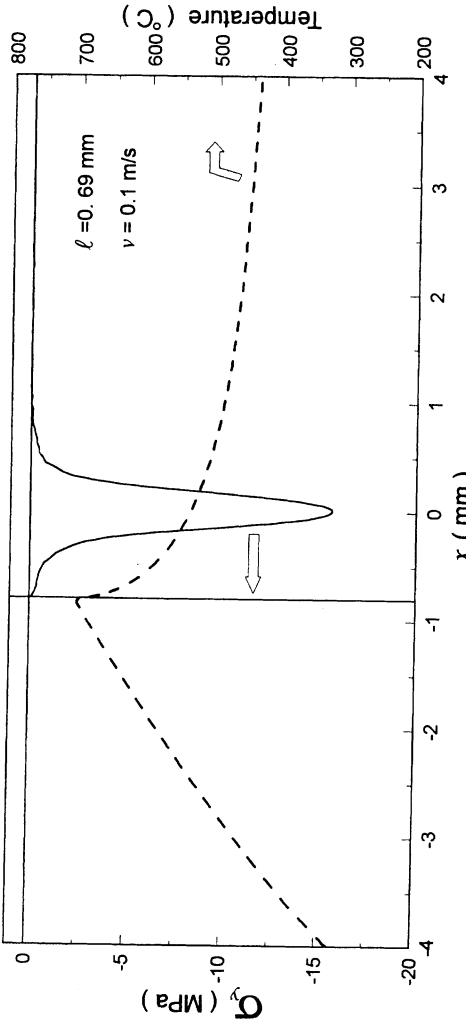

Figure 15. *Temperature and stress profiles at the interface for a roller velocity of 0.1 m/s.*

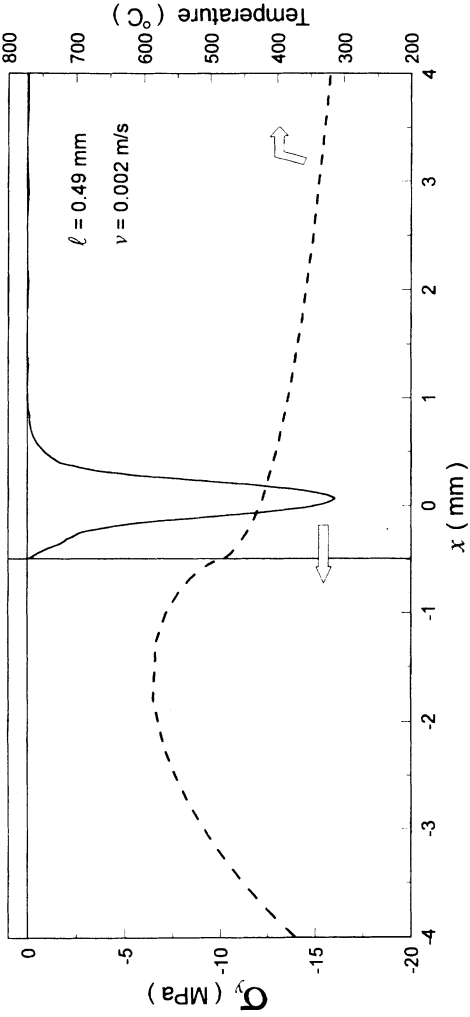

Figure 16. *Temperature and stress profiles at the interface for a roller velocity of 0.002 m/s.*

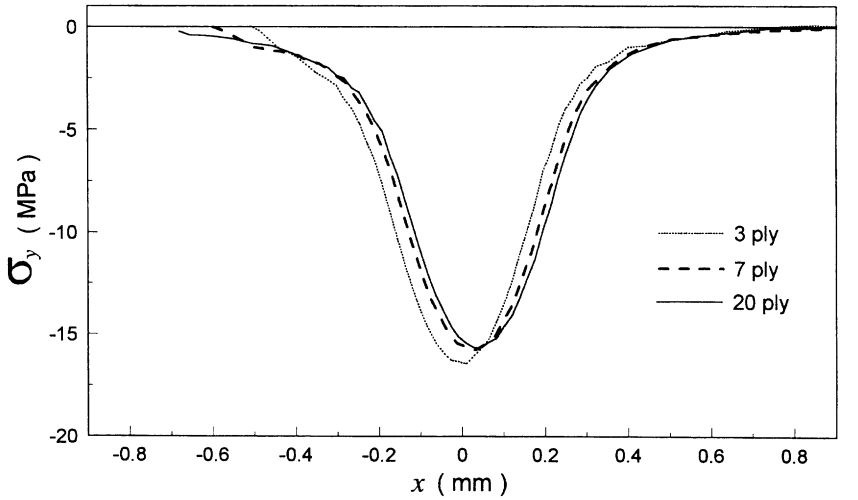

Figure 17. *The effect of laminate thickness on the stress distribution at the interface.*

laminate thickness been made. The analysis is applicable to the rolling of a slab of any thickness. Figure 17 shows the stress distribution at the interface for different laminate thicknesses. Total vertical force applied on the roller is the same for all the cases. The x-location of the peak stress changes slightly with the laminate thickness as the theoretical results also indicate (Figure 10). The smaller the sheet thickness, the more severe and the more localized stresses become. However, the effect of thickness quickly dies out after the first few layups. If the force applied on the roller is reduced for thin laminates, more uniform stress distributions can be obtained at ply-interfaces. It should also be noted that for materials having stiffness lower than APC-2, this effect is more apparent.

5. CONCLUSIONS

In this study, a stress analysis of the tape placement process has been carried out, and the effects of the process parameters on the stress field resulting from the roller force have been investigated.

Roller-induced normal stresses were found to be quite concentrated at the tape-laminate interface. Stresses decayed to zero values while the interface was still above the melting temperature of the polymer matrix. In order to maintain the pressure at the interface until the glass transition temperature is reached, application of a secondary roller or a compaction shoe was advised.

Small rollers induced very concentrated stress distributions at the interface and thus led to a shorter time available for consolidation. Therefore, larger roller diameters are more favorable to consolidation.

Thickness of the laminate affects the stress distribution. Higher and more concentrated stresses were induced in thin laminates. By controlling the roller force throughout the placement process, uniform stress distributions at ply-interfaces can be obtained.

At high roller speeds, time spent under the roller-induced high stresses was quite short. Consolidation in this case may not be complete. On the other hand, at low roller speeds, high temperature levels are not possible due to thermal degradation. Although the time spent under the roller-induced high stresses was longer, the interface experienced low temperatures. Since consolidation is a temperature-driven process, low temperatures may result in incomplete consolidation. It can then be concluded that there exists an optimum roller velocity that represents a compromise between these two conflicting effects.

NOMENCLATURE

$a(T)$ = shift factor
$[A]$ = matrix relating element strains to element nodal displacements
$[C]$ = matrix relating stresses to strains
d = depth of indentation
e_i = error coefficients
F_r = normal force
F_s = frictional force
F_y = total vertical force applied on the roller
$\{F\}$ = nodal force vector
g = convergence factor
h = thickness of the laminate
$[H]$ = effective thermal force vector
$[K]$ = stiffness matrix
l = the distance between the nip point and the y axis
S_{ij} = creep compliance
R = roller radius
t = thickness of the tape
T_{base} = base temperature for thermal strains
T_0 = base temperature for the shift factor
u_x = x component of the displacement
u_y = y component of the displacement
v_x = velocity of the roller
w = width of the tape
α_{ii} = thermal expansion coefficients
$\{\delta\}_r$ = element nodal displacement vector
$\{\delta\}_n$ = element nodal displacement vector
e^*_{ii} = thermal strain
θ = the angle between tape and laminate
μ = friction coefficient
ξ = pseudo time

ACKNOWLEDGEMENTS

This paper is based on the work supported by The Scientific and Technical Research Council of Turkey (TUBITAK) and also under the Office of Naval Research Grant N00014-92-J-1846 with Dr. Yapa D. S. Rajapakse as the Program Director.

APPENDIX A: NUMERICAL INTEGRATION OF THE CONSTITUTIVE EQUATIONS

Rewriting the constitutive equation for shear strain given in Equation (2), we have

$$\varepsilon_6(t) = \int_0^t S_{66}(\xi(t) - \xi'(\tau)) \frac{\partial \sigma_6(\tau)}{\partial \tau} d\tau \tag{A.1}$$

where *pseudo-time*, ξ, is related to the real time by

$$\xi = \int_0^t a[T(x_i, \eta)] d\eta \tag{A.2}$$

where $a(T)$ is the shift factor.

Consider the path of the material occupying the element n as depicted in Figure A.1. If the integral in Equation (A.2) is reduced to a series of finite time increments, the following equation is obtained:

$$\xi_n = \sum_{i=1}^{n-1} \frac{1}{2} \{a[T(i+1)] + a[T(i)]\} (t_{i+1} - t_i) \tag{A.3}$$

where

$$t_{i+1} - t_i = \frac{1}{2} \frac{a_{i+1} + a_i}{v} \tag{A.4}$$

a_i being the horizontal length of the mesh i.

Applying integration by parts to Equation (A.1), one obtains

$$\varepsilon_6(t) = \sigma_6(\tau) S_{66}(\xi(t) - \xi'(\tau))\Big|_0^t - \int_0^t \sigma_6(\tau) \frac{\partial S_{66}(\xi(t) - \xi'(\tau))}{\partial \tau} d\tau \tag{A.5}$$

then,

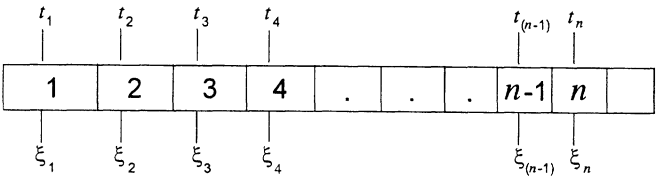

Figure A.1. *Real and pseudo time intervals for the element* n.

$$\varepsilon_6(t) = \sigma_6(t)S_{66}(0) - \sigma_6(0)S_{66}(\xi(t)) - \int_0^t \sigma_6(\tau)\frac{\partial S_{66}(\xi(t)-\xi'(\tau))}{\partial\tau}d\tau \quad \text{(A.6)}$$

Integrating Equation (A.6), by finite differences in time increments t_i or $\xi_i(t_i)$ ($i = 1,2, \ldots, n$), where $t_i = 0$ and $t_n = t$, and utilizing the second mean value theorem, one obtains

$$\varepsilon_6(t_n) = \sigma_6(t_n)S_{66}(0) - \sigma_6(0)S_{66}(\xi(t_n))$$

$$-\frac{1}{2}\sum_{r=1}^{n-1}[\sigma_6(t_{r+1}) + \sigma_6(t_r)][S_{66}(\xi_n - \xi_{r+1}) - S_{66}(\xi_n - \xi_r)] \quad \text{(A.7)}$$

By following the above procedure for ε_2, Equation (2) can be reduced to the following form:

$$\begin{Bmatrix}\varepsilon_1(t_n)\\ \varepsilon_2(t_n)\\ \varepsilon_6(t_n)\end{Bmatrix} = \sum_{r=1}^{n}\begin{bmatrix}d_{11}^{nr} & d_{12}^{nr} & 0\\ d_{12}^{nr} & d_{22}^{nr} & 0\\ 0 & 0 & d_{66}^{nr}\end{bmatrix}\begin{Bmatrix}\sigma_1(t_r)\\ \sigma_2(t_r)\\ \sigma_6(t_r)\end{Bmatrix} + \begin{Bmatrix}\varepsilon_1^*(t_n)\\ \varepsilon_2^*(t_n)\\ 0\end{Bmatrix} \quad \text{(A.8)}$$

or

$$\{\varepsilon\}_n = \sum_{r=1}^{n}[D]_{nr}\{\sigma\}_r + \{\varepsilon^*\}_n$$

where

$$d_{11}^{nr} = \begin{cases} 0 & r \neq n \\ S_{11} & r = n \end{cases} \quad \text{(A.9)}$$

$$d_{12}^{nr} = \begin{cases} 0 & r \neq n \\ S_{12} & r = n \end{cases} \quad \text{(A.10)}$$

$$d_{22}^{nr} = \begin{cases} -\frac{1}{2}\{S_{22}(\xi_n) + S_{22}(\xi_n - \xi_2) & r = 1, \quad n \neq 1 \\ \frac{1}{2}\{S_{22}(\xi_n - \xi_{r-1}) - S_{22}(\xi_n - \xi_{r+1})\} & 1 < r < n \\ S_{22}(\xi_1) & r = n = 1 \\ \frac{1}{2}\{S_{22}(\xi_1) + S_{22}(\xi_n - \xi_{n-1})\} & r = n \neq 1 \end{cases} \tag{A.11}$$

$$d_{66}^{nr} = \begin{cases} -\frac{1}{2}\{S_{66}(\xi_n) + S_{66}(\xi_n - \xi_2)\} & r = 1, \quad n \neq 1 \\ \frac{1}{2}\{S_{66}(\xi_n - \xi_{r-1}) - S_{66}(\xi_n - \xi_{r+1})\} & 1 < r < n \\ S_{66}(\xi_1) & r = n = 1 \\ \frac{1}{2}\{S_{66}(\xi_1) + S_{66}(\xi_n - \xi_{n-1})\} & r = n \neq 1 \end{cases} \tag{A.12}$$

Then, the form of (A.8) is converted to that of Equation (9), in which stress is the dependent variable. The inversion is done by the following numerical procedure:

$$\begin{aligned} \{\sigma\}_1 &= [D]_{11}^{-1}(\{\varepsilon\}_1 - \{\varepsilon^*\}_1) \\ \{\sigma\}_2 &= [D]_{22}^{-1}(\{\varepsilon\}_2 - \{\varepsilon^*\}_2 - [D]_{21}\{\sigma\}_1) \\ \{\sigma\}_3 &= [D]_{33}^{-1}(\{\varepsilon\}_3 - \{\varepsilon^*\}_3 - [D]_{31}\{\sigma\}_1 - [D]_{32}\{\sigma\}_2) \\ &\cdots\cdots\cdots\cdots\cdots\cdots\cdots\cdots\cdots\cdots\cdots\cdots\cdots\cdots\cdots\cdots \\ &\cdots\cdots\cdots\cdots\cdots\cdots\cdots\cdots\cdots\cdots\cdots\cdots\cdots\cdots\cdots\cdots \\ \{\sigma\}_n &= [D]_{nn}^{-1}(\{\varepsilon\}_n - \{\varepsilon^*\}_n - \sum_{r=1}^{n-1}[D]_{nr}\{\sigma\}_r) \end{aligned} \tag{A.13}$$

After substituting the values for $\{\sigma\}_r$ and rearranging the terms, we obtain

$$\begin{Bmatrix} \sigma_1(t_n) \\ \sigma_2(t_n) \\ \sigma_6(t_n) \end{Bmatrix} = \sum_{r=1}^{n} \begin{bmatrix} c_{11}^{nr} & c_{12}^{nr} & 0 \\ c_{12}^{nr} & c_{22}^{nr} & 0 \\ 0 & 0 & c_{66}^{nr} \end{bmatrix} \begin{Bmatrix} \varepsilon_1(t_r) - \varepsilon_1^*(t_r) \\ \varepsilon_2(t_r) - \varepsilon_2^*(t_r) \\ \varepsilon_6(t_r) \end{Bmatrix} \tag{A.14}$$

APPENDIX B: THERMAL STRAINS WITHIN A FINITE ELEMENT

Using the bilinear shape functions [25], the temperature state within a rectangular element can be expressed as follows:

$$T(x,y)=[N_1(x,y) \quad N_2(x,y) \quad N_3(x,y) \quad N_4(x,y)]\begin{Bmatrix} T_1 \\ T_2 \\ T_3 \\ T_4 \end{Bmatrix} \tag{B.1}$$

If the thermal expansion coefficients are not temperature dependent, thermal strains in the element r can be expressed as

$$\begin{aligned} \varepsilon_1^*(x,y) &= \alpha_{11}(T(x,y)-T_0)=\alpha_{11}(N_1T_1^r+N_2T_2^r+N_3T_3^r+N_4T_4^r-T_0) \\ \varepsilon_2^*(x,y) &= \alpha_{22}(T(x,y)-T_0)=\alpha_{22}(N_1T_1^r+N_2T_2^r+N_3T_3^r+N_4T_4^r-T_0) \\ \varepsilon_6^*(x,y) &= 0 \end{aligned} \tag{B.2}$$

where T_1^r, T_2^r, T_e^r and T_4^r are the node temperatures as shown in Figure B.1.

However, if they are temperature dependent as in the case of APC-2, thermal strains are given through

$$\varepsilon_{kl}^* = \int_{T_0}^{T_f} \alpha_{kl}(T)dT \tag{B.3}$$

where α_{kl} are the coefficients of thermal expansion, T_0 is the base and T_f is the present temperature. Using the trapezoidal rule, the above integration can be reduced into the following form:

$$\varepsilon_{kl}^* = \sum_{k=1}^{M}[\alpha_{kl}(T_i)+\alpha_{kl}(T_{i-1})]\frac{T_f-T_0}{2M} \tag{B.4}$$

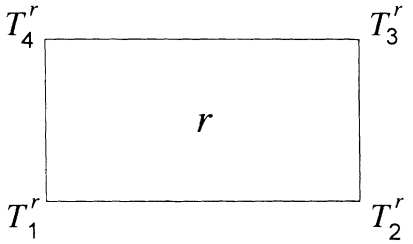

Figure B.1. *The element r and its nodal temperatures.*

or

$$\varepsilon_{kl}^{*} = \alpha_{kl}'(T_f - T_0) \tag{B.5}$$

Equation (B.2) then becomes

$$\begin{aligned}
\varepsilon_1^*(x,y) &= \alpha_{11}'(T(x,y) - T_0) = \alpha_{11}'(N_1 T_1^r + N_2 T_2^r + N_3 T_3^r + N_4 T_4^r - T_0) \\
\varepsilon_2^*(x,y) &= \alpha_{22}'(T(x,y) - T_0) = \alpha_{22}'(N_1 T_1^r + N_2 T_2^r + N_3 T_3^r + N_4 T_4^r - T_0) \\
\varepsilon_6^*(x,y) &= 0
\end{aligned} \tag{B.6}$$

REFERENCES

1. Roychowdhury, S. and S. G. Advani. 1991. "An Experimental Investigation of Consolidation in Thermoplastic Filament Winding," *Composites Manufacturing,* 2(2):97–104.
2. Sarrazin, H. and G. S. Springer. 1995. "Thermochemical and Mechanical Aspects of Composite Tape Laying," *Journal of Composite Materials,* 29(14):1908–1942.
3. Lynch, F. de S. 1969. "A FInite Element Method of Viscoelastic Stress Analysis with Application to Rolling Contact Problems," *International Journal for Numerical Methods in Engineering,* 1:379–394.
4. Batra, R. C., M. Levinson and E. Betz. 1976. "Rubber Covered Rolls—The Thermoviscoelastic Problem. A Finite Element Solution," *International Journal for Numerical Methods in Engineering,* 10:767–785.
5. Hunter, S. C. 1961. "The Rolling Contact of a Rigid Cylinder with a Viscoelastic Half Space," *Journal of Applied Mechanics,* 28:611–617.
6. Morland, L. M. 1962. "A Plane Problem of Rolling Contact in Linear Viscoelastic Theory," *Journal of Applied Mechanics,* 29:345–352.
7. Margetson, J. 1971. "Rolling Contact of a Smooth Viscoelastic Strip between Rotating Rigid Cylinders," *International Journal of Mechanical Sciences,* 13(3):207–215.
8. Margetson, J. 1972. "Rolling Contact of a Rigid Cylinder over a Smooth Elastic or Viscoelastic Layer," *Acta Mechanica,* 13(1-2):1–9.
9. Morland, L. M. 1967. "Exact Solutions for Rolling Contact between Viscoelastic Cylinders," *The Quarterly Journal of Mechanics and Applied Mathematics,* 20:73–82.
10. Kalker, J. J. 1991. "Viscoelastic Multilayered Cylinders Rolling with Dry Friction," *Journal of Applied Mechanics,* 58(3):666–679.
11. Wang, G. 1989. "Rolling Contact with Dry Friction for Two Viscoelastic Cylinders," *Zeitschrift fur Angewandte Mathematik und Mechanik,* 69(5):T501–T503.
12. Wang, G. and K. Knothe. 1993. "Stress Analysis for Rolling Contact between Two Viscoelastic Cylinders," *Journal of Applied Mechanics,* 60(2):310–317.
13. Batra, R. C. 1977. "Cold Sheet Rolling, the Thermoviscoelastic Problem. A Numerical, Solution," *International Journal for Numerical Methods in Engineering,* 11:671–682.
14. Bapat, C. N. and R. C. Batra. 1984. "Finite Plane Strain Deformations of Nonlinear Viscoelastic Rubber-Covered Rolls," *International Journal for Numerical Methods in Engineering,* 20:1911–1927.
15. Oden, J. T. and T. L. Lin. 1986. "On the General Rolling Contact Problem for Finite Deformations of a Viscoelastic Cylinder," *Computer Methods in Applied Mechanics and Engineering,* 57:297–367.

16. Cogswell, F. N. 1992. *Thermoplastic Aromatic Polymer Composites,* Butterworth-Heinemann Ltd.
17. Xiao, X. 1989. "Studies of the Viscoelastic Behavior of a Thermoplastic Resin Composite," *Composite Science and Technology,* 34:163–182.
18. Xiao, X. R. 1994. "Characterization and Modeling of Nonlinear Viscoelastic Response of PEEK Resin and PEEK Composites," *Composites Engineering,* 4(7):681–702.
19. Horoschenkoff, A. 1990. "Characterization of the Creep Composites J_{22} and J_{66} of Orthotropic Composites with PEEK and Epoxy Matrices Using the Nonlinear Viscoelastic Response of the Neat Resins," *Journal of Composite Materials,* 24:879–891.
20. Morland, L. W. and E. H. Lee. 1960. "Stress Analysis for Linear Viscoelastic Materials with Temperature Variation," *Transactions of the Society of Rheology,* 4:233–263.
21. Shapery, R. A. 1967. "Stress Analysis of Viscoelastic Composite Materials," *Composite Materials,* 1:228–267.
22. Christensen, R. M. 1982. *Theory of Viscoelasticity,* Academic Press.
23. Briscoe, B. J. 1986. "Interfacial Friction of Polymer Composites. General Fundamental Principles," in *Friction and Wear of Polymer Composites,* Composite Material Series 1, Klaus Friedrich, ed., Elsevier, pp. 25–60.
24. Hahn, H. T. and M. Levinson. 1974. "Indentation of an Elastic Layer(s) Bonded to a Rigid Cylinder—II. Unidirectional Slipping with Friction," *International Journal of Mechanical Science,* 16:503–514.
25. Yang, T. Y. 1986. *Finite Element Structural Analysis,* Prentice-Hall.
26. Sommez, F. O. 1995. "Modeling of the Thermoplastic Composite Tape Placement Process," Ph.D. Thesis, UCLA, Los Angeles.
27. Ross, C. T. F. 1990. *Finite Element Methods in Engineering Science,* Ellis Horwood.
28. Ha, S. K., Q. Wang and F.-K. Chang. 1991. "Modeling the Viscoplastic Behavior of Fiber-Reinforced Thermoplastic Matrix Composites at Elevated Temperatures," *Journal of Composite Materials,* 25:334–374.
29. Xiao, X. 1989. "Studies of the Viscoelastic Behavior of a Thermoplastic Resin Composite," *Composites Science and Technology,* 34:163–182.
30. Sichina, W. "Time-Temperature Superpositioning Studies of Thermoplastic Composites," ANTEC '88, pp. 1139–1142.
31. Ogale, A. A. and R. L. McCullough. 1987. "Influence of Microstructure of Elastic and Viscoelastic Properties of Polyether Ether Ketone," *Composites Science and Technology,* 30: 185–201.
32. Ma, C.-C.M, H.-C. Hsia, W.-L. Liu and J.-T. Hu. 1987. "Thermal and Rheological Properties of Poly(phenylene sulfide) and Poly(ether etherketone) Resins and Composites," *Polymer Composites,* 8(4):256–264.
33. D'Amore, A., A. Pompo, J. Mijovic and L. Nicolais. 1994. "The Kinetics of Volume Relaxation and Related Property Changes during Physical Aging of Poly(ether ether ketone) (PEEK)," *Composite Structures,* 27:45–49.
34. Yoon, K. J. and C. T. Sun. 1991. "Characterization of Elastic-Viscoplastic Properties of an AS4/PEEK Thermoplastic Composite," *Journal of Composite Materials,* 25:1277–1296.
35. Xiao, X. R. and A. H. Cardon. 1990. "Temperature Dependence of the Viscoelastic Behavior of PEEK Resin and PEEK Composite," *Development and Design with Advanced Materials,* Elsevier Science Publishers, pp. 79–87.
36. D'Amore, A., A. Pompo, P. Netti, E. Masi and L. Nicolais. 1993. "Non-Linear Viscoelastic Behavior of Poly-Ether-Ether-Ketone (PEEK) and PEEK-Based Composites," *Journal of Reinforced Plastics and Composites,* 12:327–340.
37. Kim, R. Y. and J. T. Hartness. 1987. "Time-Dependent Response of AS-4/PEEK Composite," *19th International SAMPE Technical Conference,* pp. 468–475.
38. Barnes, J. A., I. J. Simms, G. J. Farrow, D. Jackson, G. Wostenholm and B. Yates. 1990. "Ther-

mal Expansion Behavior of Thermoplastic Composite Materials," *Journal of Thermoplastic Composite Materials,* 3:66–80.

39. Barnes, J. A. 1993. "Thermal Expansion Behavior of Thermoplastic Composites," *Journal of Material Science,* 28:4974–4982.
40. Moore, D. R., I. M. Robinson, N. Zahlan and F. J. Guild. 1989. "Mechanical Properties for Design and Analysis of Carbon Fibre Reinforced PEEK Composite Structures," *Materials and Processing—Move into the 90's,* pp. 167–185.
41. Sonmez, F. O. and H. T. Hahn. 1997. "Process Modeling of Heat Transfer and Crystallization for Thermoplastic Composite Tape Placement," *Journal of Thermoplastic Composite Materials,* 10(3):198–240.
42. Leterrier, Y. and C. G'sell. 1994. "Formation and Elimination of Voids during the Processing of Thermoplastic Matrix Composites," *Polymer Composites,* 15(2):101–105.
43. Muzzy, J. D. 1988. "Processing of Advanced Thermoplastic Composites," in *The Manufacturing Science of Composites, Proceedings of Manufacturing International,* T. G. Gutowski, ed., 4:27–39.
44. Muzzy, J., L. Norpoth and B. Varughese. 1989. "Characterization of Thermoplastic Composite for Processing," *SAMPE Journal,* 25(1):367–375.
45. Enders, M. L. 1990. "Developments in Thermoplastic Filament Winding," *22nd International SAMPE Technical Conference,* pp. 88–97.